DFRA/DFIS – A New Technology for Battery Instrumentation and Testing

by

Keith S. Champlin, Ph.D.
Professor Emeritus
University of Minnesota
5437 Elliot Avenue South
Minneapolis, Minnesota 55417

Kevin Bertness
Vice President, Research & Development, Midtronics, Inc.
7000 Monroe Street
Willowbrook, Illinois 60521
kbertness@midtronics.com

DFRA/DFIS – A New Technology for Battery Instrumentation and Testing

Keith S. Champlin, Ph. D.
Professor Emeritus, University of Minnesota
5437 Elliot Avenue South
Minneapolis, MN 55417 USA
champlin@ece.umn.edu

Kevin Bertness
Vice President, Research & Development, Midtronics, Inc.
7000 Monroe Street
Willowbrook, IL 60521 USA
k.bertness@midtronics.com

1. Introduction

Predicting a battery's performance without actually discharging it has long been a topic of great interest. Battery conductance [1-8] and impedance magnitude [8,9] have proven very useful in predicting cranking performance and relative capacity. However, both conductance and impedance magnitude comprise only a single ac quantity measured at a single frequency. Far more information is contained in the complete spectrum of the battery's complex immittance, (i.e., either complex impedance or complex admittance) measured over a range of frequencies. A big challenge is to accurately capture this information and reduce it to a relatively small number of useful parameters.

We describe a new immittance measuring technique, "Digital Frequency Response Analysis" (**DFRA**), which, when combined with a new analysis methodology, "Discrete Frequency Immittance Spectroscopy" (**DFIS**), evaluates previously unavailable battery parameters. The battery is excited with a periodic current, and its complex impedance or admittance is determined with **DFRA**. By measuring at **n** discrete frequencies and combining the **2n** measured quantities using **DFIS**, one determines elements of a **2n**-element equivalent-circuit model of the battery. These elements represent actual physical and/or electrochemical processes, and their values have potential for yielding:

- State of charge (in percent)
- Absolute charge (in reserve capacity minutes, amp-hours, or coulombs)
- Percent capacity (based upon standardized ratings)
- Load-current capability (cold-cranking amps)

- Internal battery temperature
- Cell uniformity ("bad" cell detection)
- Good/Bad Assessment (state of "health")

This new technique appears to show promise for applications in battery manufacturing, quality control, field service work, battery installation and maintenance, "smart" battery charging, remote battery monitoring, battery-vehicle "fuel gauges", and electrochemical research.

2. Digital Frequency Response Analysis (DFRA)

DFRA is closely related to the conventional "frequency response analysis" (**FRA**) method of impedance measurement [10-12]. It is fully disclosed in U.S. Patents **6,002,238** and **6,172,483**. Figure **1** shows a block diagram illustrating typical **DFRA** architecture.

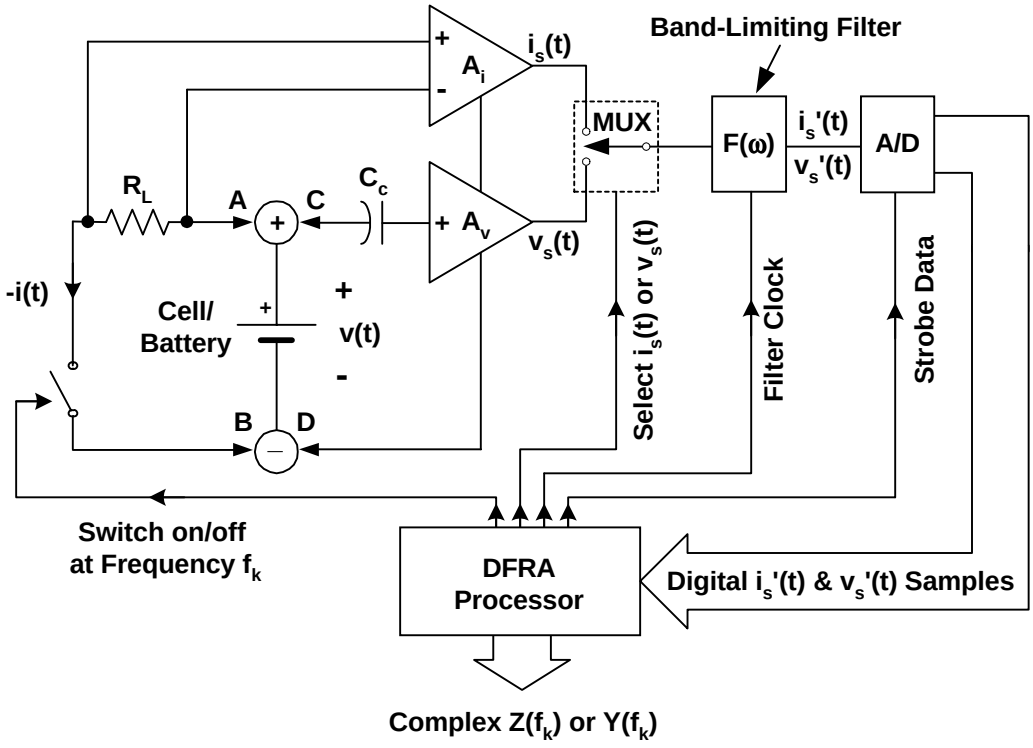

Figure 1. Typical DFRA measuring architecture

In the implementation shown in Figure **1**, a load current is switched on and off by the **DFRA** processor to produce a square wave battery current $i(t)$ at frequency f_k. This time-

varying current passes through the cell/battery at contacts **A** and **B.** Capacitively-coupled contacts **C** and **D** sense the resulting time-varying voltage across the cell/battery, $v(t)$. Linear circuitry amplifies two signals. One signal, $i_s(t)$, is proportional to the time-varying battery current. The other, $v_s(t)$, is proportional to the time-varying component of battery voltage. These two signals are multiplexed together and individually selected by the **DFRA** processor for presentation to the input of band-limiting filter $F(\omega)$. The two band-limited signals at the output of the filter, either $i_s'(t)$ or $v_s'(t)$, are sampled by the **A/D** converter at **M** evenly spaced times over a period $T_k = 1/f_k$. Digital representations of these two synchronously-sampled, band-limited, signals are inputted to the **DFRA** processor.
The **DFRA** processor acquires data for a total of **N** periods and then uses the **MxN** digital samples of each signal to evaluate the complex immittance of the cell/battery at frequency f_k.

A conventional frequency response analyzer (**FRA)** employs hardware devices to multiply an input signal by reference sinusoidal and cosinusoidal signals and performs hardware integrations of the resulting products. With **DFRA**, the **DFRA** processor employs software to perform these same functions. Using this new technique, the complex impedance of cells and batteries can be routinely measured with errors of less than **0.1%**.

3. Typical Admittance Spectra

Measured spectra of real and imaginary parts of complex admittance $Y = 1/Z = G + jB$ of a typical flooded **12V SLI** automotive battery, measured over the frequency range from **5 Hz** to **1000 Hz,** are plotted in Figures **2** and **3**, respectively.

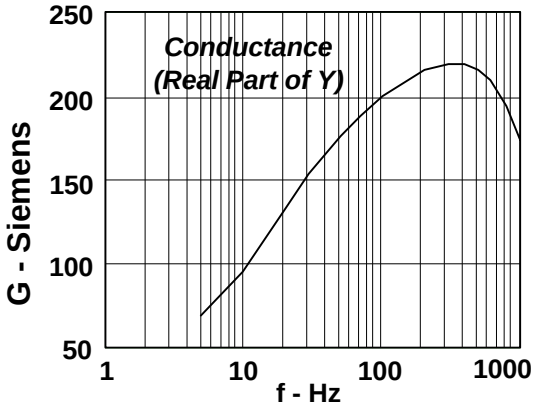

Figure 2. Conductance spectrum of 12V SLI battery

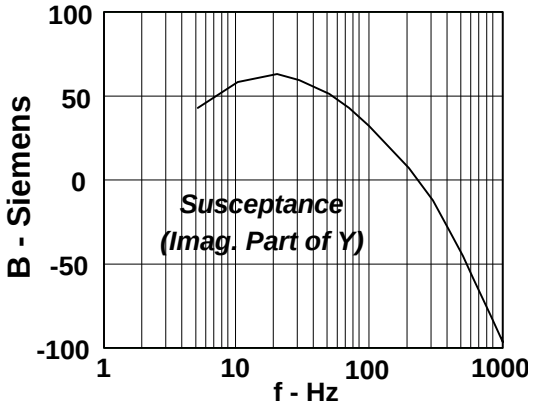

Figure 3. Susceptance spectrum of 12V SLI battery

Considerable information about the battery is expressed in spectral plots such as those disclosed in Figures **2** and **3**. One sees, e.g., that the battery passes through series resonance near **250 Hz,** being capacitive **(B>0)** below **250 Hz** and inductive **(B<0)** above. However, most of the information contained in such immittance spectra is very subtle, and not at all obvious from the plots. Hence, the need for **DFIS**.

4. Discrete Frequency Immittance Spectroscopy (DFIS)

DFIS is closely related to the research discipline known as "electrochemical impedance spectroscopy" (**EIS**) [11,12]. However, it differs from conventional **EIS** in the type of circuit models employed and the way that the circuit elements are evaluated. **DFIS** is fully disclosed in U.S. Patent **6,037,777**. Figure **4** shows a block diagram illustrating architecture combining **DFIS** methodology with the immittance measuring circuitry of Figure **1**.

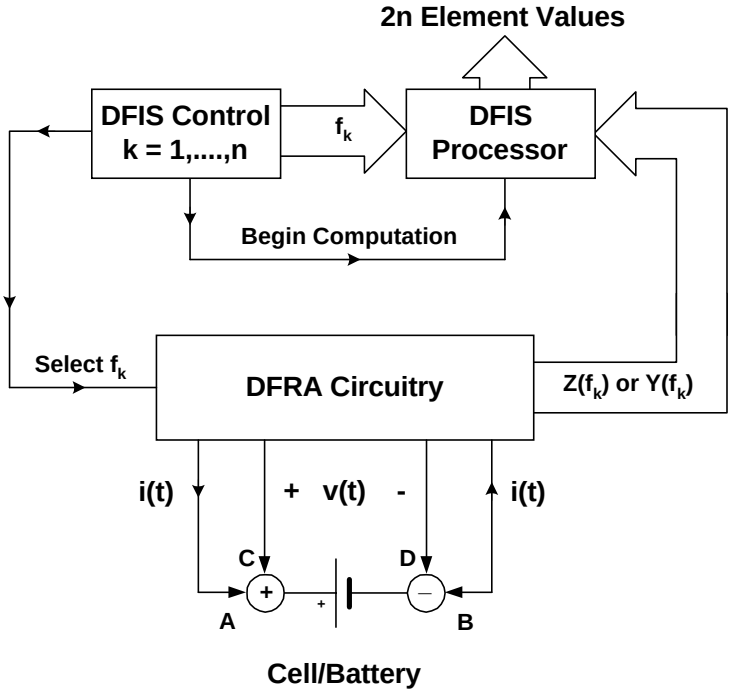

Figure 4. Typical DFIS Architecture

The **DFIS** controller commands the **DFRA** circuitry to determine real and imaginary parts of complex immittance at a discrete frequenciy $\mathbf{f_k}$ and repetitively increments **k** until **k = n**. From the resulting **2n** measured quantities, the **DFIS** processor directly calculates values of the **2n** elements of the generic equivalent-circuit model shown in Figure **5**.

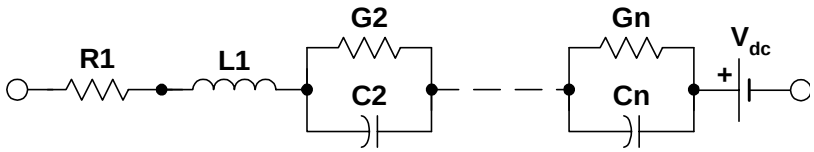

Figure 5. Generic DFIS Circuit Model

The results of a **DFIS** computation with **n = 2** are shown in Figure **6**. The input data for this computation are those disclosed in Figures **2** and **3** at discrete frequencies $\mathbf{f_1 = 5\ Hz}$ and $\mathbf{f_2 = 1000\ Hz}$. Two widely-separated time constants are noted.

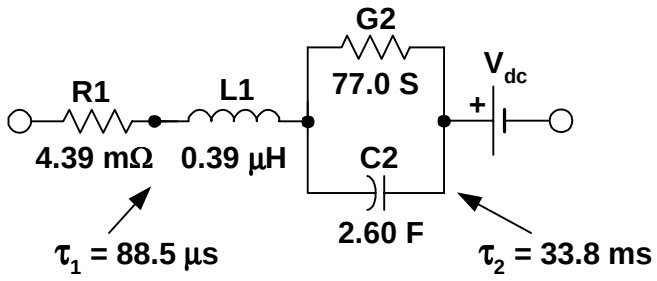

Figure 6. DFIS results for n = 2

Using well-known analytical methods, the complex admittance of the circuit model of Figure **6** was calculated as a function of frequency. Figures **7** and **8** show the results of these calculations plotted along with the experimental curves of Figures **2** and **3** for comparison.

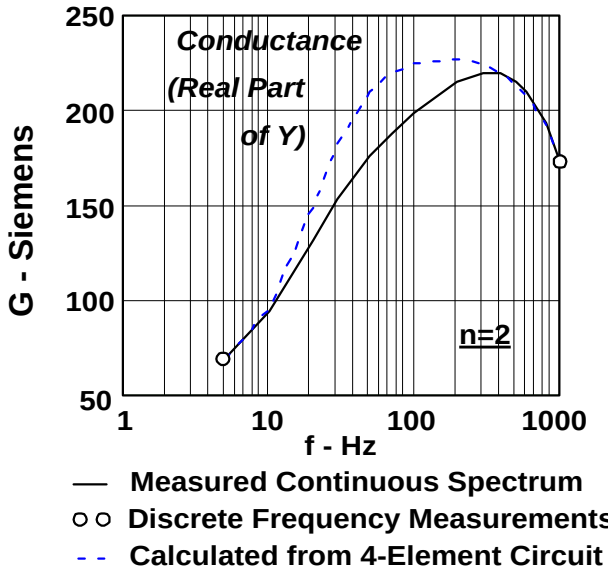

Figure 7. Measured G compared with G from model of Figure 6.

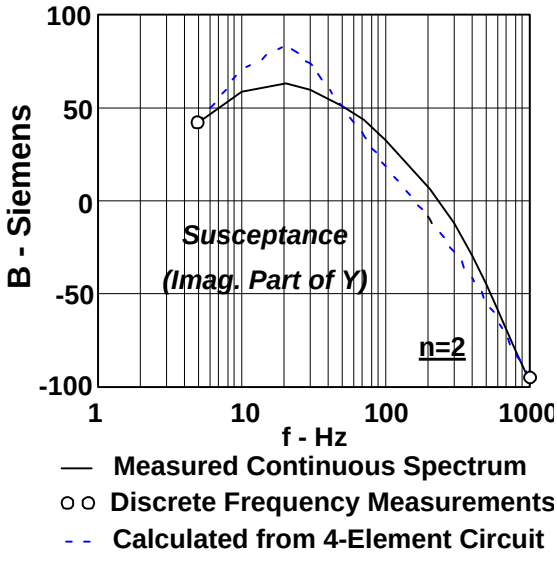

Figure 8. Measured B compared with B from model of Figure 6.

As would be anticipated, theoretical and experimental curves agree exactly at the two discrete measurement frequencies, **5 Hz** and **1000 Hz**. However, away from these frequencies the agreement is poor. Thus, the model of Figure **6** does not adequately represent the battery over this frequency range.

A second **DFIS** computation was performed with **n = 3** using the experimental data of Figures **2** and **3** evaluated at the three frequencies $\mathbf{f_1 = 5\ Hz}$, $\mathbf{f_2 = 70\ Hz}$, and $\mathbf{f_3 = 1000\ Hz}$. The results of this computation are displayed in Figure **9**. Plots comparing experimental curves with those calculated from the Figure **9** model are disclosed in Figures **10** and **11**.

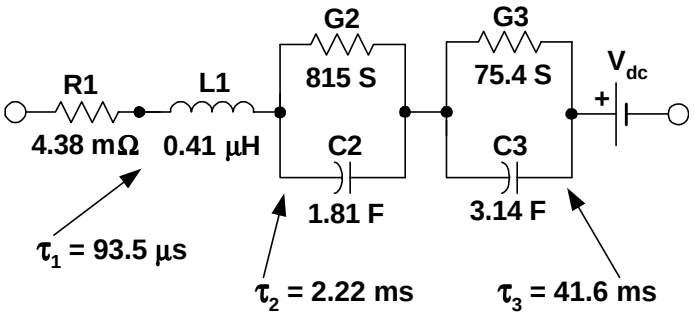

Figure 9. DFIS results for n = 3

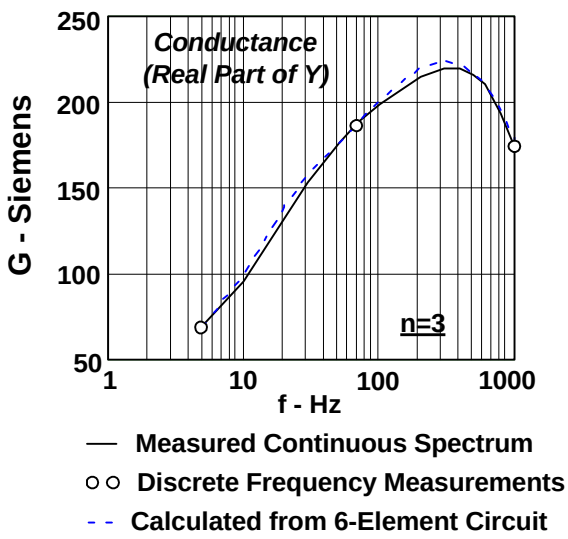

Figure 10. Measured G compared with G from model of Figure 9.

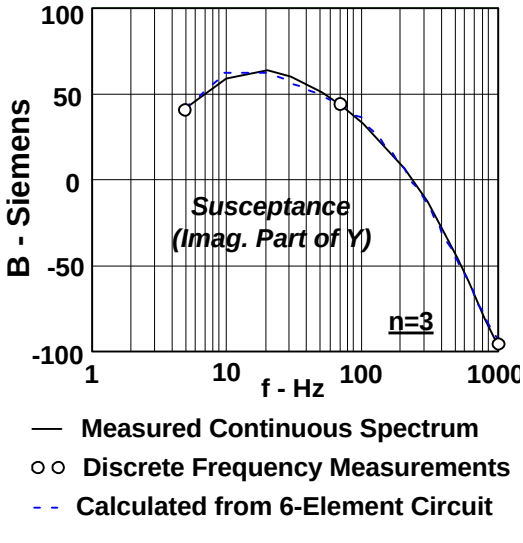

Figure 11. Measured B compared with B from model of Figure 9.

Once again the experimental and theoretical curves agree exactly at the discrete measurement frequencies. Away from these frequencies however, the agreement is now also very good. Such agreement proves the circuit model of Figure **9** to be an excellent representation of the battery over the complete frequency range from **5 Hz** to **1000 Hz**. Accordingly, the six element values that are disclosed in Figure **9** contain virtually the same information as the complete spectral plots of Figures **2** and **3**. However, they embody this information in a much more concise form that is far easier to store, analyze, and manipulate than the spectral plots from which they were derived.

5. Some Experimental Results

The following results are typical **DFRA/DFIS** measurements performed on dozens of flooded and **VRLA** batteries in an ongoing experimental program at Midtronics, Inc. These data were all obtained with **n = 3**: $\mathbf{f_1 = 5\ Hz}$, $\mathbf{f_2 = 50\ Hz}$, and $\mathbf{f_3 = 500\ Hz}$.

Figure **12** discloses variation of the three time-constants as charge is removed from a **50** ah battery in **4.6** amp-hour steps. One notes that the time-constants remain widely separated throughout the entire range of discharge. This behavior is typical of all batteries studied so far.

Figure **13** shows capacitance **C2** in Farads as charge is removed from a **60** ah battery in approximately **6** amp-hour increments. One observes that **C2** decreases monotonically as charge is removed. This suggests that **C2** might be used to determine the absolute charge in either amp-hours, reserve capacity minutes, or coulombs, that is contained in a battery. Such a **DFRA/DFIS** implementation would comprise a true battery "fuel gauge".

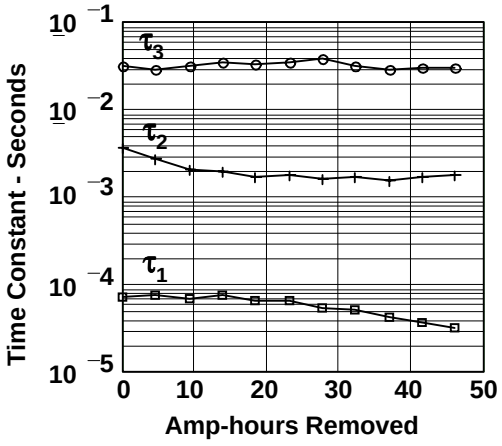

Figure 12. Time-constants vs ah removed

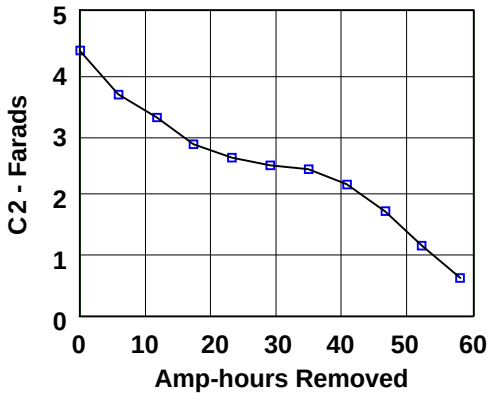

Figure 13. Variation of C2 with ah removed

Figure **14** is a plot of amp-hour capacity as a function of **C2** at full-charge for six different batteries from the same manufacturer. The experimental amp-hour capacities were determined from actual timed-discharge tests. One sees that the points lie fairly close to a straight line. Such close agreement with a linear relationship implies that full-charge amp-hour capacity could possibly be determined from **DFIS** measurements without ever actually discharging the battery.

Conductance **G3** is plotted as a function of amp-hours removed from a **60** amp-hour battery in Figure **15**. One observes that **G3** approaches zero (i.e., **R3 = 1/G3** approaches infinity) at both full-charge and at full-discharge; and that **G3** reaches maximum (**R3** reaches minimum) near **50%** state of charge **(SOC)**. This observed variation of **G3** closely follows an expression of the form –

$$G3 = K(G1)(SOC)(1 - SOC) \qquad (1)$$

where **SOC** ranges from **0.93** to **0.22** in Figure **15**. This result is typical of all of the batteries tested and could lead to the development of a new method for determining **SOC**.

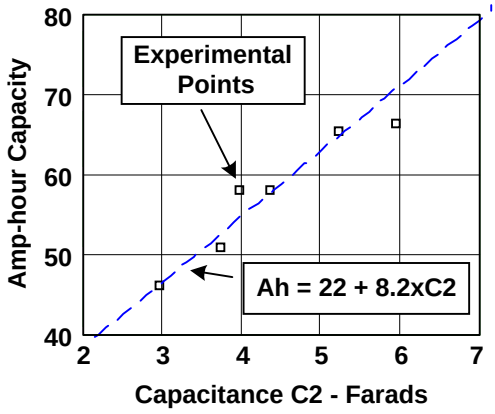

Figure 14. Full-charge ah capacity vs C2

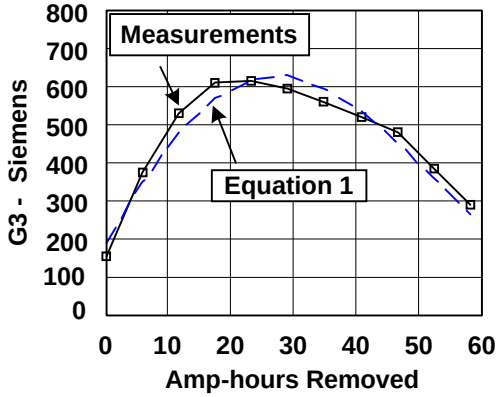

Figure 15. G3 as function of ah removed

6. Interpretation

Resistance **R1** is believed to describe the current-induced drop in electric potential across the metal connectors, plates, separators, and electrolyte – with the "lion's share" of **R1** due to the electrolyte. The reciprocal of this resistance, **G1**, is directly related to load-test

current. Inductance **L1** appears to simply describe energy stored in the battery's magnetic field, with no electrochemical component of **L1** yet observed.

The **G3-C3** subcircuit is believed to describe *chemical* (Faradaic) processes at the negative plates. This interpretation is consistent with the observed value and temperature variation of τ_3 and with the fact that equilibrium reaction rates should be proportional to both the number of sites available for the discharge reaction and to the number available for the charge reaction. The **G2-C2** subcircuit is believed to describe *electrical* processes at the negative plates with **C2** being the *double-layer capacitance.* In this interpretation, the observed variation of **C2** with charge (Fig. **13**) describes variation of the number of metallic **Pb** sites with the battery's charge. These two negative-plate subcircuits add in series because the total electrochemical potential difference at the metallic terminals (Figure **16)** is the *sum* of all *chemical* potential differences and all *electrical* potential differences in the battery [13].

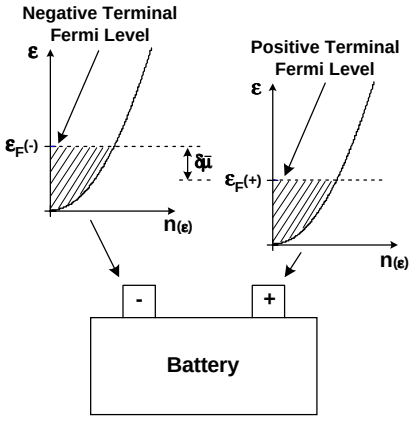

Figure 16. Total Electrochemical Potential Difference

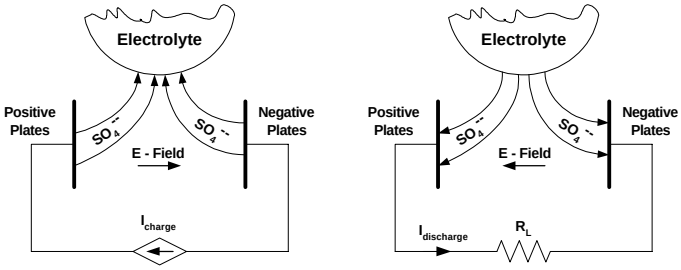

Figure 17. E-field aids migration of SO_4^- ions to/from - plates but opposes it to/from + plates

Why the *negative* plates? As seen in Figure **17**, the electric field aids migration of the (negative) sulphate ions to/from the negative plates but opposes it to/from the positive plates. Accordingly, electrochemical reactions at the positive plates are diffusion-limited and are many orders of magnitude slower than the reactions at the negative plates.

It is interesting to note that Shukla, et al. [14], evaluated a circuit similar to Figure **9** (without **L1)** by analyzing very slow transient behavior. They even observed variation of one of their resistive elements with **SOC** similar to the variation disclosed in Figure **15**.

However, the time-constants that they observed, **25.67 s** and **332 s**, are many times longer than those reported herein. It is therefore very possible that they were observing electrochemical processes occurring at the *positive* plates, while the experiments reported herein describe much faster processes occurring at the *negative* plates.

6. Conclusions

DFRA/DFIS represents a fundamentally new approach to battery instrumentation. This technology appears to have many potential applications in battery manufacturing, quality control, field testing and service work, cell matching, battery installation and maintenance, "smart" battery charging, remote battery monitoring, thermal runaway detection, battery-vehicle "fuel gauges", and electrochemical research.

References

1. K. S. Champlin, "Dynamic Method for Storage Battery Diagnostic Testing", 1975 SAE Off-Highway Meeting, Milwaukee WI, (Sept 8-11, 1975), Paper 750758.

2. D. O. Feder, T. G. Croda, K. S. Champlin, and M. J. Hlavac, "Field and Laboratory Studies to Assess the State of Health of Valve-Regulated Lead Acid Batteries. Part I - Conductance/Capacity Correlation Studies", Intelec 92, pp. 218-233.

3. M. J. Hlavec, D. O. Feder, T. G. Croda, and K. S. Champlin, "Field and Laboratory Studies to Assess the State-of-Health of Valve-Regulated Lead acid and Other Battery Technologies. Part II - Further Conductance/Capacity Correlation Studies", Intelec 93, pp. 375-383.

4. D. O. Feder and M. J. Hlavec, "Analysis and Interpretation of Conductance Measurements Used to Assess the State-of-Health of Valve-Regulated Lead Acid Batteries. Part III - Analytical Techniques", Intelec 94, pp. 282-291.

5. M. J. Hlavec and D. O. Feder, "VRLA Battery Monitoring Using Conductance Technology. Part IV - On Line State of Health Monitoring and Thermal Runaway Detection/Prevention", Intelec 95, pp. 284-291.

6. M. J. Hlavec and D. O. Feder, "VRLA Conductance Monitoring. Part V - Strategies for VRLA Battery Testing and Monitoring in Telecom Operating Environments", Intelec 96, pp. 632-639.

7. D. C. Cox, D. O. Feder, M. E. Troy, M. J. Hlavec, J. Dunn, and W. J. Popp, "Midpoint Conductance Technology Used in Telecommunication Stationary Standby Battery Applications", Intelec 97, pp. 695-702.

8. M. Kniveton and A. I. Harrison, "Impedance/Conductance Measurements as an Aid to Determining Replacement Strategies", Intelec 98, pp. 297-301.

9. G. J. Markle, "Ac Impedance Testing For Valve Regulated Cells", Intelec 92, pp. 212-217.

10. See, e. g., H. Allison, "Frequency Response Analyzer", U. S. Patent 4,322,806, Mar. 30, 1982. See also website: www.solartron.com.

11. D. Robinson, "Electrochemical Impedance Spectroscopy in Battery Development and Testing", *Batteries International*, (April 97), pp. 59 - 63.

12. See, e.g., J. Ross MacDonald, *Impedance Spectroscopy*, J. Wiley and Sons, Inc. (1987)

13. See, e. g., A. J. Bard and L. R. Faulkner, *Electrochemical Methods*, J. Wiley and Sons, Inc, (1980), pp. 60, 633.

14. A. K. Shukla, V. G. Kumar, N. Munichandraiah, T. S. Srinath, "A Method to Monitor Valve-Regulated Lead Acid Cells", *Journal of Power Sources*, 74, (1998), pp. 234-239.